Available online at www.sciencedirect.com
ScienceDirect
Applied Catalysis B: Environmental 80 (2008) 313–320
APPLIED CATALYSIS B: ENVIRONMENTAL
www.elsevier.com/locate/apcatb

Photocatalytic properties of visible-light enabling layered titanium oxide/tin indium oxide films

Kee-Rong Wu [a,*], Ting-Pin Cho [b]

[a] Department of Marine Engineering, National Kaohsiung Marine University, Kaohsiung 811, Taiwan
[b] Metal Industries Research and Development Centre, Treatment Processing & Equipment Section, Kaohsiung 811, Taiwan

Received 21 April 2007; received in revised form 22 September 2007; accepted 25 September 2007
Available online 9 October 2007

Abstract

Visible-light enabling titanium oxide/tin indium oxide (TiO_2/ITO) thin films deposited on unheated glass slides with prolonged deposition duration were investigated in this study. Structural properties characterized by X-ray diffraction (XRD), Raman spectra and scanning electron microscopy (SEM) showed typical polycrystalline structure with primary anatase phase along with elongated pyramid-like grains lying on the film surface and densely packed columnar structure from cross-sectional profile. The XRD preferential peak of (2 1 1) and the Raman peak intensity at $\sim$640 cm^{-1} dramatically increased without noticeable broadening and shift as the deposition time was prolonged beyond 2 h. This implies that more perfectly crystalline structure, less internal stress, and comparatively larger grains were obtained by this technique. The $Ti2p_{3/2}$ and O1s XPS peaks shifted toward higher binding energy suggest that the local chemical state was influenced by the prolonged deposition duration in the film, which resulted in red shift of absorption threshold into visible-light region. Under ultra-violet (UV) and visible-light illumination, the visible-light enabling film exhibited the best photocatalytic activity on MB degradation with the rate-constant of about 0.231 h^{-1}. Hydrophilic conversion rate was estimated to be 8.14×10^{-3} deg^{-1} min^{-1} and long-term UV-induced hydrophilicity of $\sim$10° in the dark storage up to 72 h was observed. In addition to its inherent characteristics of the layered TiO_2/ITO structure on hole/electron separation, all these could be attributed to more perfectly formed crystalline structure, densely packed columnar crystals and the surface roughness along with its enlarged surface area.

Keywords: Titanium oxide/tin indium oxide (TiO_2/ITO) films; Visible-light; Hydrophilicity

1. Introduction

Titanium dioxide (TiO_2), extensively used as an environmentally harmonious and clean photocatalyst, has attracted much attention in the past two decades, because of its various merits, such as optical and electronic properties, low cost, high photocatalytic activity, chemical stability and non-toxicity [1]. In general, the generation of electron–hole pairs following ultra-violet (UV) light excitation on TiO_2 catalysts affords the possibility of both reductive reactions by electrons and oxidative reaction by holes [2]. Oxidation takes place in the presence of oxygen. An electron from the conduction band reduces molecular oxygen to its radical anion, which then reacts further resulting in the oxidation of contaminants. In addition to its photocatalytic activity, TiO_2 thin films also exhibit a hydrophilic property with a contact angle of less than 5° after UV illumination. This phenomenon, together with the photocatalytic activity, has enabled these films to be used, for example, in self-cleaning windows, tiles and anti-fogging mirrors.

Up to the present, visible-light sensitive TiO_2 photocatalyst has been prepared by a hydrolytic process by calcination of hydrolysis product of $Ti(SO_4)_2$ [3], tetra-butyl titanate ($Ti(OBu)_4$) solution [4], or acidified $TiCl_3$ [5] with ammonia solution heated in a furnace at 400–450 °C in dry air. Ihara et al. have reported that the N-doped TiO_2 catalysts showed visible-light photocatalysis by decomposing acetone under irradiation of blue-light-emitting diodes (BLED) [3]. The synthesized N-doped rutile catalysts showed very good photocatalytic activity on the degradation of methylene blue (MB) under bright sunlight in comparison to the commercial rutile power sample [5]. We previously reported that the TiO_2 films prepared on unheated glass substrates by twin direct current (DC) magnetron sputtering, due to high sputtering power density,

* Corresponding author. Tel.: +886 73617141x3218; fax: +886 73629500.
E-mail address: krwu@mial.nkmu.edu.tw (K.-R. Wu).

0926-3373/$ – see front matter © 2008 Published by Elsevier B.V.
doi:10.1016/j.apcatb.2007.09.045

without the need for post-heat treatment or calcinations at high temperatures, exhibited very good crystallinity with high deposition rate, nanohardness and strong adhesive strength [6].

In this paper, we report the successive deposition of layered TiO_2/ITO thin films using twin DC sputtering technique. We found that the layered TiO_2/ITO films exhibited remarkable self-cleaning properties including weak-light hydrophilicity and visible-light induced photocatalysis. Notably the layered TiO_2/ITO thin films were more efficient photocatalytic films than equivalent ones under illumination of various light sources.

2. Experimental procedure

2.1. Sputtering system

Layered TiO_2/ITO films were deposited on unheated glass slide (25 mm × 75 mm × 1 mm) substrates using an in house pulse-arc plasma-aided twin DC magnetron sputtering system in a chamber with dimensions W300 mm × D300 mm × H400 mm, which was operated in a class 1000 clean room. This four-magnetron system consists of opposite vertical twin targets each of dimensions 400 mm × 100 mm × 6 mm. In this work, the ITO films were initially deposited onto unheated rotating glass substrates using a pair of vertical ITO targets, 90 wt.% In_2O_3 and 10 wt.% SnO_2 on one side of the chamber. The total pressure was set to 1.2×10^{-3} Pa, whereas the partial sputtering pressure, 0.11 Pa, was maintained as the reactive argon–oxygen gas mixture (2% oxygen) was introduced. After the desired thickness of ITO film was formed, the substrate holder was rotated 180° towards the other side of another pair of vertical titanium targets (99.5% purity) without opening the chamber for the formation of TiO_2 top layers. The total pressure was still set at 1.2×10^{-3} Pa, whereas the partial sputtering pressure, 0.27 Pa, was maintained during the overlaid TiO_2 deposition. The target-to-substrate distance was kept at 60 mm during the layered TiO_2/ITO thin film deposition. In Table 1, we denote vi-TiO_2 for the visible-light enabling TiO_2/ITO thin films in which the "*i*" (1, 2, 3) represents the deposition hours for preparing the overlaid TiO_2 thin films and the DC-sputtered TiO_2 (pure TiO_2) thin film as a reference was prepared at presumably the optimal conditions.

2.2. Characterization of the samples

The crystal structures of the layered vi-TiO_2 films were analyzed by X-ray diffractometry (XRD) using a BEDE D1 diffractometer operating with Cu Kα radiation at 40 kV, 50 mA and an angle of incidence of 4°. The Raman spectra were measured with a JOBIN-YVON T64000 Micro-PL/Raman spectroscopy using He-Cd 325 nm laser excitation source. The topography of samples was analyzed using an atomic force microscope (AFM, SPI 3800N, Seiko Instruments Inc.) with a scan resolution of 512 × 512 pixels over an area of 500 nm × 500 nm. The microstructure of the films was investigated by a scanning electron microscope (JEOL JSM-6700F) at an operating voltage of 5 kV.

Table 1
Some sputtering conditions used in this study

Sample	Sputtering time (min)		Sputtering current (A)	
	ITO	Overlaid TiO_2	ITO	Overlaid TiO_2
TiO_2	–	50	–	3.6
v1-TiO_2	12	60	1.0	3.1
v2-TiO_2	12	120	1.0	3.0
v3-TiO_2	12	180	1.0	3.0

The stoichiometry of the film surface was characterized using an X-ray photoelectron spectroscope (XPS, VG ESCA Scientific Theta Probe) with an Al Kα (1486.6 eV). The base pressure in the analysis chamber was approximately 4×10^{-6} Pa. The spectra of the Ti2p and O1s peaks were calibrated with respect to the C1s peak at the energy of 284.6 eV. Etching was performed by using Ar^+ ion source on the sample surface with a voltage of 15 kV and about 0.3 mA for 60 s.

A UV spectrophotometer (Hitachi UV-2001) was used to measure the light transmittance of the samples, where a blank glass slide was used as reference. The wettability of the film upon UV irradiation was determined from changes in the water contact angles using a commercial contact angle meter (FTA 200, First Ten Angstrom) at a laboratory temperature of about 25 °C. An average water contact angle was obtained from at least five measurements at various points on the same sample. A set of black-light lamps (365 nm) with average light intensity of 1.0 mW/cm^2, measured by a UV radiometer (UVX Radiometer, UVX-25), was employed as the light source.

2.3. Photocatalytic degradation of methylene blue

The photocatalytic activity of the samples was evaluated by immersing the samples of size 25 mm × 65 mm into 30 ml aqueous MB solution of concentration 10 ppm in a visible-light cylindrical Pyrex reactor under illumination of various light sources. Sets of light-emitting-diodes of various spectrum, blue LED (BLED, $420 < \lambda < 530$ nm), green LED (GLED, $470 < \lambda < 600$ nm) and red LED (RLED, $600 < \lambda < 670$ nm), nm), were chosen as the visible-light sources. The average intensity of the BLED, GLED and RLED were about 1.0, 1.6 and 1.8 mW/cm^2, with the peaked wavelength at 470, 544 and 630 nm, respectively, measured by a spectrophotometer (Ocean Optics USB2000). A black light lamp (365 nm) with average light intensity of 1.2 mW/cm^2, measured by a UV radiometer (UVX Radiometer, UVX-25), was used as the UV-light source.

A background of MB degradation was always carried out under the specified irradiation with a blank sample. The photocatalytic degradation rate under the same irradiation was calculated by subtracting the background concentration. The photocatalyzed MB solutions were kept in the dark for hours to release leuco-methylene blue (LMB) prior to carrying out the transmittance measurements [7]. The transmittance of the solution was measured by a Shimadzu UV-1601 spectrometer at a wavelength of 664 nm. Subjecting to no stirring motion, all experiments were carried out in solution of natural pH (6.80) at a laboratory temperature of about 25 °C.

3. Results and discussion

3.1. X-ray diffraction

A layer of TiO_2 film was firstly sputtered onto the glass slide substrate, as a binder layer to prevent from peeling, at a lower sputtering power and in an oxygen-rich gas mixture. The residual stress of the deposited films was estimated by XRD spectra using the relationship, $\beta \cos\theta/\lambda = 1/D + 4\varepsilon \tan\theta/\lambda$, proposed by Rickerby et al. [8], in which θ is the angle of XRD peak corresponding to the (n k l) plane of the film defined by Bragg's law, λ is the wavelength (0.1541 nm with a Cu Kα source) of X-ray beam, D is the crystallite diameter for each phase and ε is the strain corresponding to the XRD peak. The crystallite diameter can be determined from the full width half maximum (FWHM) of anatase (1 0 1) diffraction according to Scherrer's equation.

As presented in Fig. 1, the characteristic XRD patterns of layered vi-TiO_2 thin films, where $i = 1$, 2, 3, that appeared primarily in the well-crystallized anatase phase with the preferential peaks of (1 0 1) and (2 1 1), and a trace of rutile phase and crystallized ITO phase with the preferential peaks of (2 2 2), (4 0 0) and (4 4 0). The peak ratio of the (4 0 0/2 2 2) was ∼0.4, yielding relatively low sheet resistance in the ITO substrates [9]. The preferential peak of (2 1 1) dramatically increased as the deposition time was prolonged beyond 2 h. It should be mentioned that the shift of the v3-TiO_2 film toward a bulk value recorded at $2\theta = 25.28^\circ$ indicates smaller residual stresses in the films due to the increased size of anatase crystallites, as shown in Table 2.

3.2. Raman spectra

Fig. 2 shows that the layered vi-TiO_2 thin films were in well-crystallized anatase phase. One can see that the v3-TiO_2 film exhibited an extremely strong intensity peak at 142–145 cm^{-1}, three mid-intensity peaks at 397, 517 and 640 cm^{-1} and a weak one at 195 cm^{-1}, which corresponded well to the Degussa P-25 film [10] or single crystal anatase TiO_2 [11]. A significant increase of peak intensity at ∼640 cm^{-1} was found to increase with the deposition duration. No distinct peak that corresponded to rutile TiO_2, such as the peak at 446 cm^{-1}, appeared. On the other hand, the v2-TiO_2 film also exhibited similar spectra with weaker intensity peaks. Preparing a TiO_2 film on a commercial ITO glass substrate by dip-coating promoted the anatase-rutile transformation and broadened and shifted peaks in the Raman spectra [12]. However, the peaks of both the v2-TiO_2 and v3-TiO_2 samples did not exhibit noticeable broadening and shift, perhaps because the layered films formed by successive deposition had more crystalline structure, less internal stress [11] and comparatively larger grains as listed in Table 2. As is well known, larger grains are associated with less blue shifting and less shifting in the Raman spectra. The above observations are also confirmed by UV–vis transmittance measurement to be discussed in the section below.

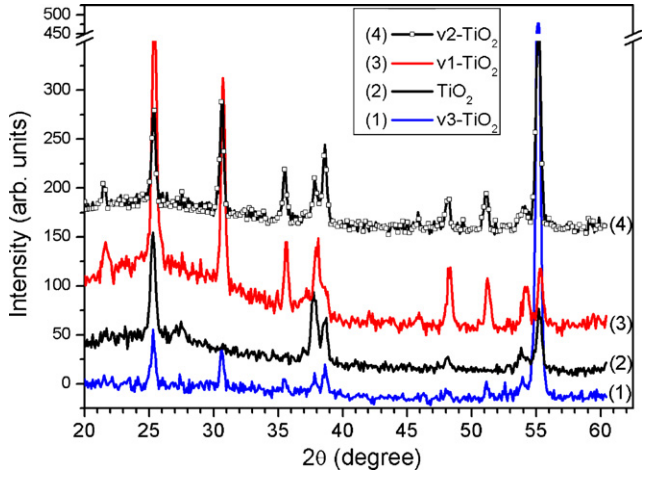

Fig. 1. XRD patterns of layered vi-TiO_2 films along with pure TiO_2 sample, where $i = 1$, 2, 3.

3.3. UV–vis transmittance

Fig. 3 shows the UV–vis transmittance spectra of the layered vi-TiO_2 films. The absorption threshold at wavelength shorter than 380 nm can be assigned to the intrinsic band gap absorption of pure anatase TiO_2 (∼3.2 eV). The layered vi-TiO_2 thin films exhibited enhanced absorption at longer than 450 nm wavelength. One can see that the v3-TiO_2 film exhibited the longest light absorption up to 600 nm wavelength among all the samples. The visible-light responsive ability revealed by the v3-TiO_2 film is similar to that of the undoped-TiO_2 prepared at relatively high substrate temperatures of about 873 K by radio frequency sputtering reported by Anpo and co-workers [13]. They deduced that the visible-light enabling absorption of the undoped-TiO_2 thin films was due to a decline of the Ti^{4+}/O^{2-} ratio inside the structure, which produced a profound effect on the electronic structure perturbation of the films. It is interesting to note that the v3-TiO_2 films deposited on unheated glass substrates appeared milky yellow and transparent. These may be the results of more oxygen vacancies due to the underlaid ITO thin film.

By preparing the layered TiO_2/ITO films, more oxygen vacancies are created due to the underlaid ITO. The oxygen vacancy states between the valence and the conduction bands are newly formed in the TiO_2 band structure. It is expected that the oxygen vacancy states take part in a new photo-excitation process. That is, the electron may be excited to the oxygen vacancy states from the valence band under with visible-light irradiation. The activation of oxygen, especially the formation of O^- ion, is considered to be very important for photocatalytic oxidation processes [14]. Therefore, it is presumed that the electrons excited to the oxygen vacancy state or the holes formed in the valence band perhaps react with O_2 or oxygen species and produce the reactive oxygen species such as O^- or atomic oxygen, which will participate in the oxidation process of photocatalysis, such as MB degradation.

3.4. SEM measurements

Fig. 4 shows the SEM surface morphology of the layered vi-TiO_2 films deposited for (a) 3 h v3-TiO_2, (b) 2 h v2-TiO_2 and

Table 2
Some sample properties obtained by XRD measurement

Sample	Residual stress (MPa)	(1 0 1) Diffraction			(2 1 1) Diffraction		
		2θ	FWHM	Diameter (nm)	2θ	FWHM	Diameter (nm)
TiO_2	−206.0	25.33	0.335	48.1	55.06	0.375	47.2
v1-TiO_2	−200.8	25.30	0.346	46.5	55.18	0.356	49.8
v2-TiO_2	−198.7	25.39	0.344	46.9	55.28	0.346	51.2
v3-TiO_2	−159.0	25.33	0.336	48.0	55.14	0.354	50.1

(c) 1 h v1-TiO_2, and (d) pure TiO_2 thin film for comparison. For the v1-TiO_2 film deposited for a shorter time of 1 h, relatively fine particles were observed. As the deposition duration increased, the diameter of TiO_2 particles increased and a prismatic top structure became dominant. As revealed by the layered v3-TiO_2 film, the surface morphology in Fig. 4(a) shows more closely aligned crystallites than those prepared at shorter deposition time. Meanwhile, cross-sectional view in Fig. 5(a) displays more closely packed columnar crystals with a prismatic-like structure observed from the layered v3-TiO_2 film. On the other hand, the v1-TiO_2 film exhibited blunt packed columnar structure in Fig. 5(c). For increasing deposition duration to 2 h (v2-TiO_2), there was little increase in the film thickness, but the surface properties and crystal structure changed significantly. These results suggest that the surface properties and crystal structure were enhanced significantly at the later stage of the TiO_2 film growth. The surface properties of the samples listed in Table 3 were obtained by AFM measurements. The specific surface area was calculated to be in the range from 1.30 (v1-TiO_2) to 1.56 (v3-TiO_2). It was known that the above-mentioned characteristics were most likely observed on TiO_2 thin films deposited at temperature not less than 600 °C [15]. It can be concluded that the prolonged deposition duration may facilitate the formation of crystallite growth with more closely packed columnar crystals and prismatic-like structure.

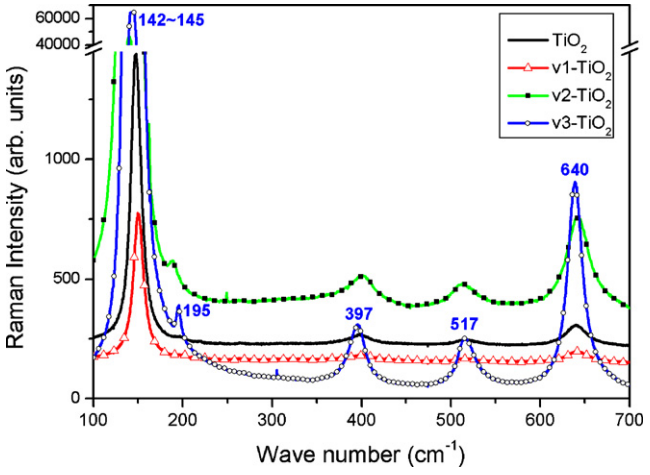

Fig. 2. Raman spectra of the layered vi-TiO_2 films presented along with pure TiO_2 sample.

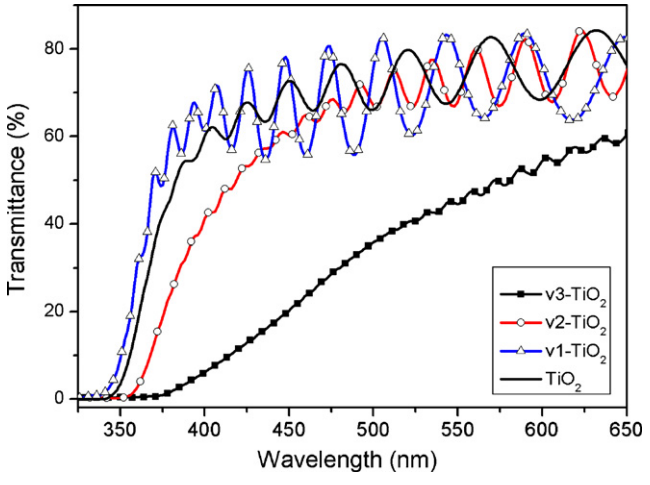

Fig. 3. Transmittance spectra of layered vi-TiO_2 films compared with pure TiO_2 thin film.

3.5. XPS analysis

The surface stoichiometry of the vi-TiO_2 films prepared at different sputtering durations was examined by XPS on both as-deposited and 60 s argon ion etched samples. The latter are presented in Figs. 6 and 7. The binding energies for the $Ti2p_{3/2}$ and the O1s spectra observed in an anatase thin film were 458.8 and 529.9 eV, respectively [16]. Accordingly, the two peaks observed at ∼458.8 and ∼464.5 eV from the layered v1-TiO_2 film in Fig. 7 are assigned to $Ti2p_{3/2}$ and $Ti2p_{1/2}$, respectively. For the layered v3-TiO_2 film, not only the $Ti2p_{3/2}$ peak but also the O1s peak was found to shift toward higher binding energy. This suggests that, in addition to more oxygen vacancies created, the local chemical state was influenced by prolonged deposition duration in the film, perhaps resulting in red shift of the absorption threshold into the visible-light region. The O1s spectra of the layered vi-TiO_2 films indicated significant shift toward the higher side of binding energy with increase of deposition duration. For the layered v3-TiO_2 film, the O1s spectrum showed a peak at ∼529.9 eV for bulk oxide ion (O^{2-}) and a shoulder that fitted into a peaks at ∼531.7 eV, which was assigned to the surface hydroxyl groups (OH^-) [17-19]. One can deduce from the O1s spectra in Fig. 6 that the layered v3-TiO_2 film possessed a great amount of OH^- at ∼531.7 eV. On the other hand, the v1-TiO_2 film showed a shoulder to the main O1s peak at higher binding energy, but with much less intensity. Nagaveni et al. pointed out that the enhanced photocatalytic activity of combustion-synthesized catalyst on MB degradation was attributed to the crystallinity, nano-size distribution of 10-12 nm, large amount of OH^- and reduced band-gap energy of

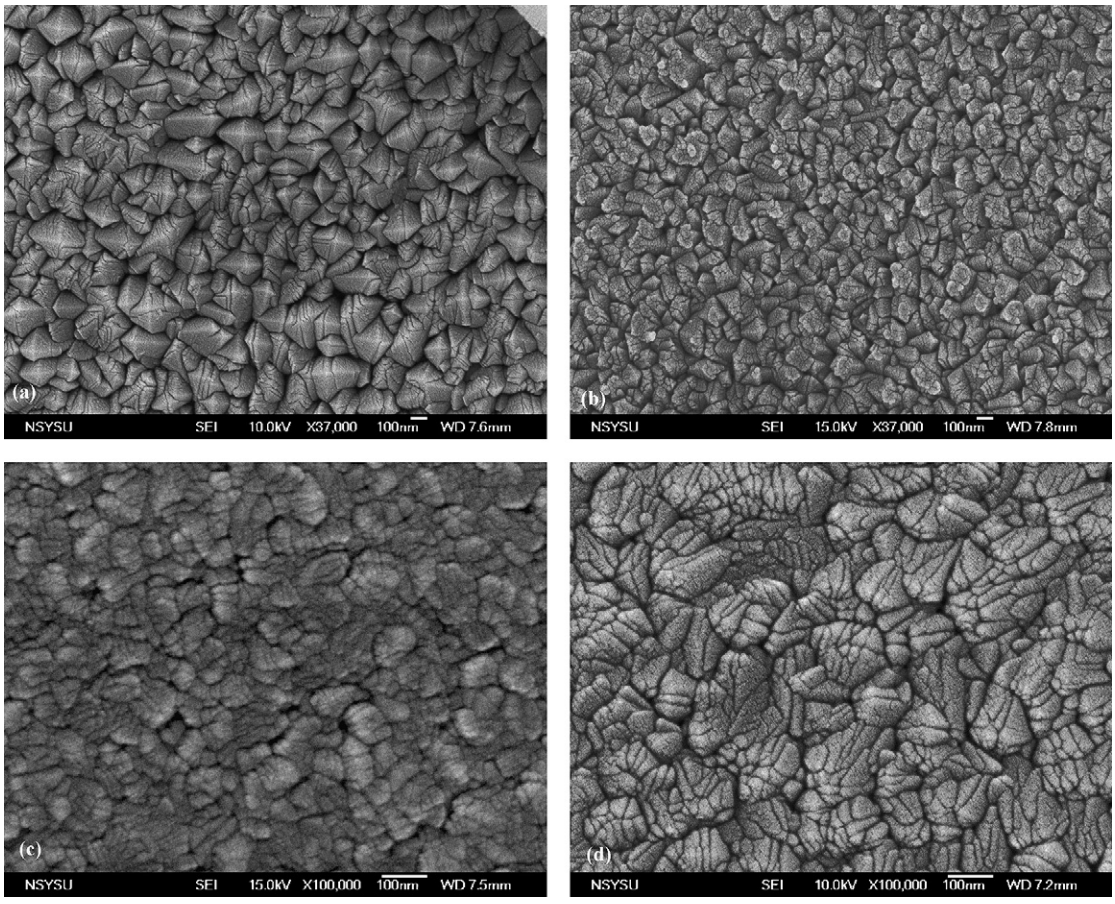

Fig. 4. Typical SEM surface morphology of layered (a) v3-TiO_2, (b) v2-TiO_2, (c) v1-TiO_2 and (d) pure TiO_2 thin films.

2.18 eV [20]. Since surface hydroxyl groups, the most abundant adsorbates, are known to play an important role in the photodegradation of organic pollutant [20] and hydrophilic conversion rate [19], it seems that these groups accept holes generated by irradiation to form surface hydroxyl radicals. Thus, they emphasized the conclusions that the better photocatalytic activity of the nanosize TiO_2 particles can be due to the increased surface hydroxyl groups. Therefore, it is expected that a greater amount of surface hydroxyl groups yield a higher degradation rate over pollutants. Thus, the layered v3-TiO_2 film contains more hydroxyl groups, which result in higher photo-induced activities in favor of better reduction rate and hydrophilic conversion rate under UV or visible-light irradiation [18–21].

3.6. Photocatalytic activity

Fig. 8 shows the photo-induced degradation of methylene blue (MB) over the layered vi-TiO_2 films irradiated by UV-365. These results indicate that MB was decomposed by a photocatalytic reaction in the presence of the vi-TiO_2 catalysts. The layered v3-TiO_2 film exhibited the best photocatalytic activity with a rate-constant of about 0.231 h^{-1}, assuming pseudo first-order reaction kinetics. The pure TiO_2 thin film displayed the least photocatalytic activity with a rate constant of about 0.036 h^{-1}, slightly inferior to sample v1-TiO_2, under UV-365 illumination. Dumitriu et al. showed that the presence of metallic Ti precipitates in the DC-sputtered TiO_2 films significantly impaired the photocatalytic activity [22]. They related the fact to the TiO_2 thin films deposited at a higher deposition rate and on colder substrates than the other sample sets. Thus, Ti precipitates in the film could become recombination sites for photo-induced charge carriers. This is one of the reasons that the layered v2-TiO_2 and v3-TiO_2, prepared at a slightly lower power and longer deposition duration, exhibited much better photo-induced activity on MB degradation under UV-365 illumination.

Under various wavelengths of visible-light illumination, i.e., BLED ($420 < \lambda < 530$ nm), GLED ($470 < \lambda < 600$ nm) and RLED ($600 < \lambda < 670$ nm), the layered v3-TiO_2 film was the most active on MB degradation among all the samples. This is shown in Fig. 9. The layered v2-TiO_2 film was relatively active under BLED and BLED illumination. Noting that the layered v3-TiO_2 film showed profound photocatalytic ability under the wavelengths longer than 600 nm, which is consistent with the UV–vis measurements shown in Fig. 3.

3.7. UV-induced hydrophilicity

Water contact angles were measured to elucidate the changes in the surface hydrophobic recovery rate under UV-365 irradiation and in the rate for the reverse process in the dark

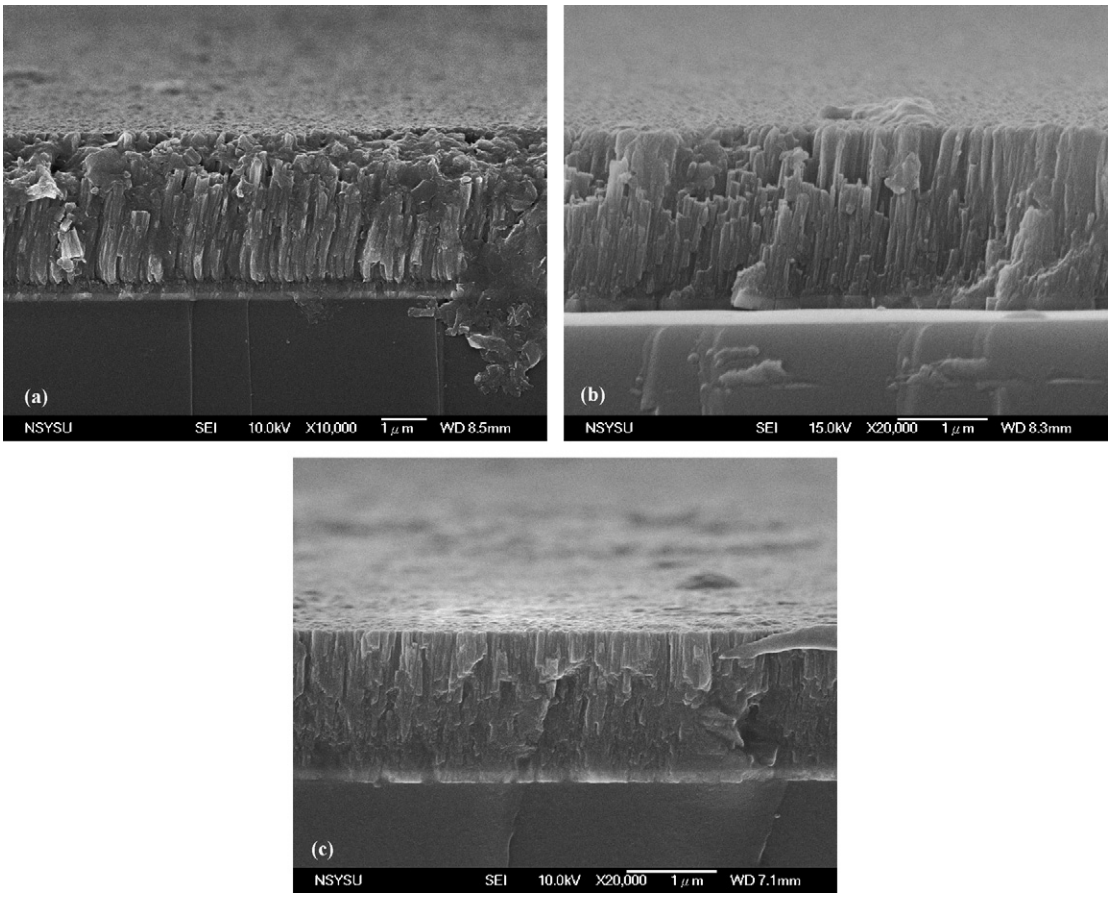

Fig. 5. Typical SEM surface and cross-sectional morphology of layered (a) v3-TiO_2, (b) v2-TiO_2 and (c) v1-TiO_2 thin films.

for the pure TiO_2, layered v2-TiO_2 and v3-TiO_2 films, as shown in Fig. 10. The hydrophobic recovery rate is defined as the ratio of the UV-induced contact angle to the initially fresh contact angle in the dark. Measurements of water contact angles for the reverse process in the dark were made when the samples were stored in the dark for a specified period. Fig. 10 reveals that the hydrophobic recovery rate for the v3-TiO_2 film decreased dramatically to 0.02 approximately. In other words, the water contact angle reached $\sim 2^\circ$ with 60 min UV illumination, compared with an initial value of 99°. On the other hand, the water contact angle for the pure TiO_2 thin film dropped initially from 89 to $\sim 8^\circ$ under 60 min UV illumination. The reciprocal of the contact angle plotted against the UV illumination duration exhibits very good linearity, as shown in Fig. 11. The slope of the straight lines, defined as hydrophilic conversion rate, was estimated to be $8.14 \times 10^{-3}\ \mathrm{deg}^{-1}\ \mathrm{min}^{-1}$ for the v3-TiO_2 film, which was compared as high as the value reported in the literature [19]. However, the slopes were only about 2.48×10^{-3} and $1.50 \times 10^{-3}\ \mathrm{deg}^{-1}\ \mathrm{min}^{-1}$ for the v2-TiO_2 and pure TiO_2 films, respectively.

The ITO thin film is of a band gap of 3.5 eV and similar band edge position to WO_3 and SnO_2. In the layered TiO_2/ITO system, the electrons that are excited to the conduction band

Table 3
Surface properties obtained by AFM measurement

Sample	TiO_2/ITO thickness (nm)	RMS roughness (nm)	Specific surface area
TiO_2	1800/–	9.2	1.20
v1-TiO_2	2050/150	17.4	1.30
v2-TiO_2	2100/200	19.8	1.39
v3-TiO_2	3600/200	35.9	1.56

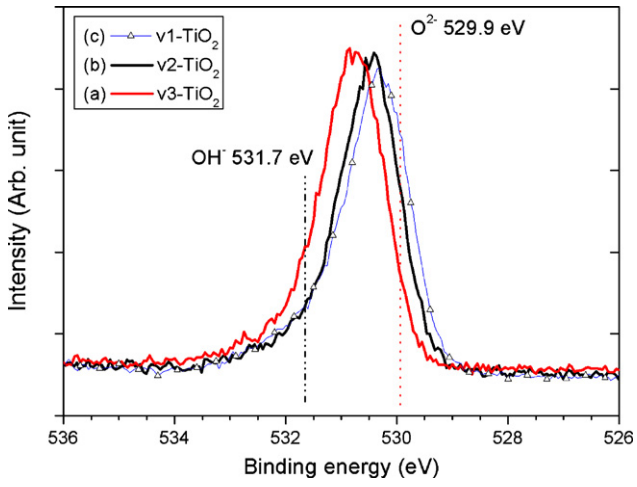

Fig. 6. O1s XPS spectra of layered (a) v3-TiO_2 (b) v2-TiO_2 and (c) v1-TiO_2 thin films after 60 s etching.

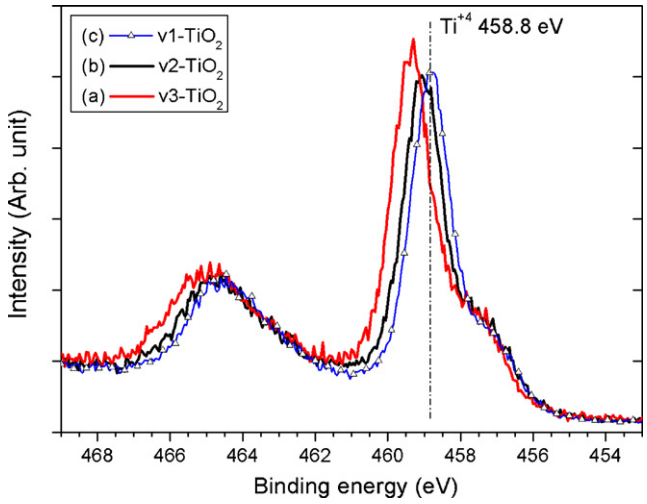

Fig. 7. O1s XPS spectra of layered (a) v3-TiO_2 (b) v2-TiO_2 and (c) v1-TiO_2 thin films after 60 s etching.

from the valence band of TiO_2 film under UV illumination are transferred along the band toward the conduction band of the ITO substrate [12]. In relation to the hybrid amorphous-WO_3/TiO_2 film [23] and doped crystalline-WO_3/TiO_2 film [24], the photo-generated holes effectively accumulate in the TiO_2 layer and the excited electrons remain in the ITO layer. The recombination of the photo-generated carriers is suppressed in the layered TiO_2/ITO film. One can deduce from the XRD patterns and the Raman spectra in Figs. 1 and 2, respectively, that the layered v3-TiO_2 film exhibited almost the same characteristics with more intensity in terms of polycrystalline structure as compared with that of the v2-TiO_2 film. Note that no noticeable rutile phase (110), which contained more bridging oxygen atoms for easy hydrophilic, was detected in both samples. This implies that the v3-TiO_2 film contains purer and more perfect crystals than that of v2-TiO_2 film. Meanwhile, the apparent contact angle θ^* on a rough surface can be evaluated by Wenzel's law, $\cos\theta^* = r\cos\theta$, where θ is the contact angle of an ideal flat homogeneous surface and r is the

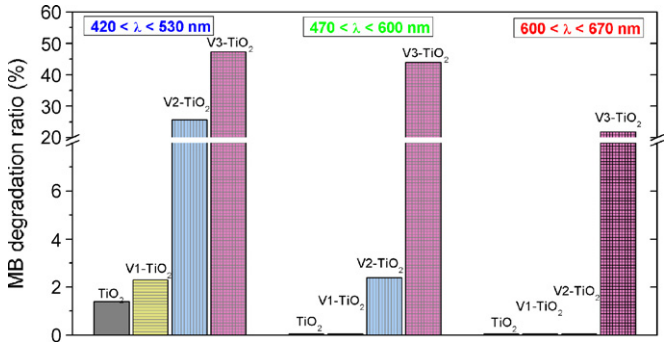

Fig. 9. Photocatalytic activity of layered vi-TiO_2 films and pure TiO_2 thin film under various visible-light sources; BLED and GLED for 24 h and RLED for 12 h.

roughness area ratio of the surface, defined as the ratio between the real surface and the projected ones, which is always greater than one ($r > 1$). Since the Wenzel's law remains valid experimentally when θ is slightly higher than 90°, the water contact angle for a rough but stoichiometric surface will be smaller than that for a smooth surface [25]. These imply that the v3-TiO_2 film having the highest RMS roughness 35.9 nm could result in the best photo-induced hydrophilicity among the samples tested, as displayed in Figs. 10 and 11. Thus, the superior photo-induced hydrophilicity of the layered v3-TiO_2 film is attributed to the well crystallized and rough overlaid TiO_2 film [26] and the role of underlaid ITO layer by successive deposition in this study.

Interestingly, the hydrophilicity of the layered v3-TiO_2 and v2-TiO_2 films in Fig. 10 was retained at ~10° for at least 72 h and at ~19° for 48 h, respectively, while the pure TiO_2 film recovered its hydrophobic state at ~80° within 30 h after turning off the UV light. This indicates that the layered v3-TiO_2 film retained some hydrophilicity during a long period of storage in the dark. This perhaps is because the excess electrons are accepted by the electron pools; hence the reductive energy generated can be stored. After the UV light is switched off, electrons that have been stored in the electron pool are injected

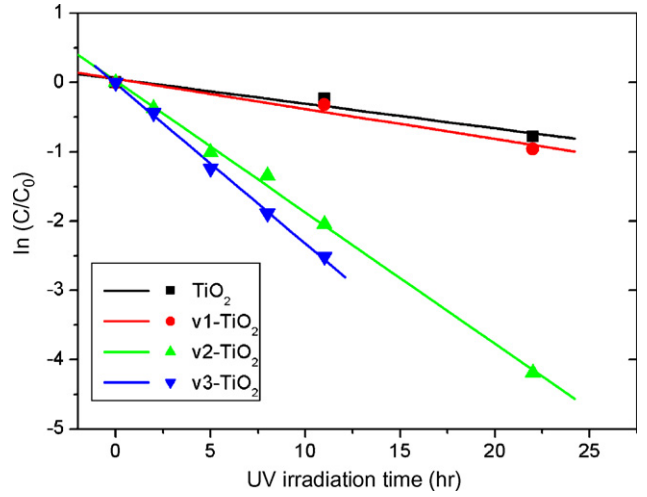

Fig. 8. Photocatalytic MB degradation of layered vi-TiO_2 films and pure TiO_2 thin film under UV-365 illumination.

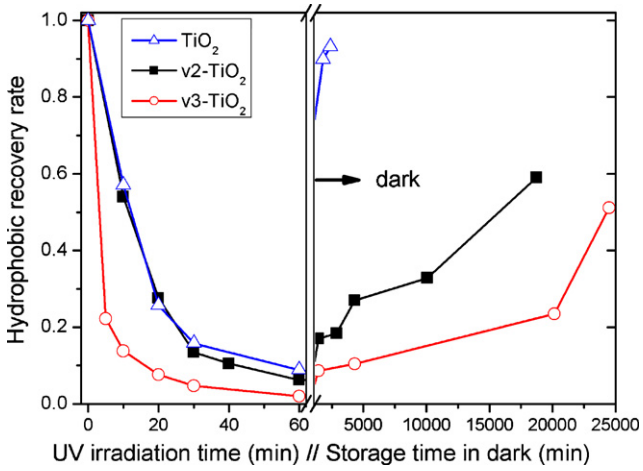

Fig. 10. Hydrophobic recovery rate of pure TiO_2, layered v2-TiO_2 and v3-TiO_2 films under UV-365 light irradiation of 1.0 mW/cm^2 intensity and thereafter storage in the dark.

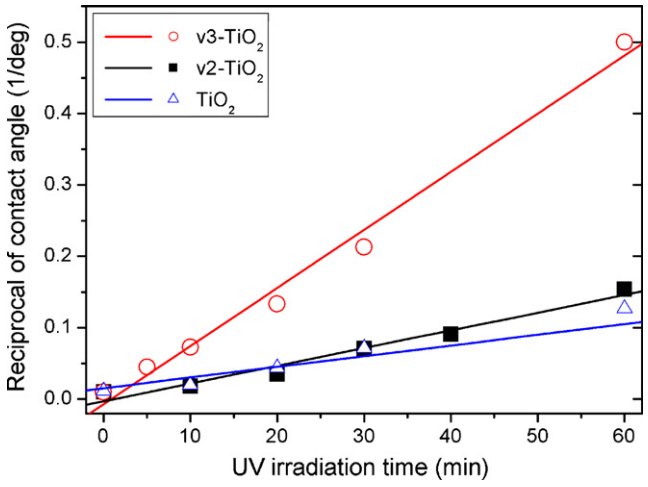

Fig. 11. Reciprocal of water contact angles of pure TiO_2, layered v2-TiO_2 and v3-TiO_2 films under UV-365 light irradiation of 1.0 mW/cm^2 intensity.

to the surface, resulting in a slow decrease of the photo-induced wettability over a long period in the dark. The columnar structure of the v3-TiO_2 film may also promote the transformation of holes or electrons, and retard the holes and electrons recombination rate.

4. Conclusions

In this study, visible-light enabling v3-TiO_2 films deposited on unheated glass slide with prolonged deposition duration were characterized by XRD, Raman spectra and SEM with respect to other samples prepared with shorter deposition. The layered v3-TiO_2 films showed typical polycrystalline structure with primary anatase phase along with elongated pyramid-like grains lying on the film surface and densely packed columnar structures on the cross-sectional image. The XRD preferential peak of (2 1 1) and the Raman peak intensity at ~640 cm^{-1} dramatically increased without noticeable broadening and shift as the deposition duration was prolonged beyond 2 h, indicating that the layered films formed by successive deposition had more perfectly crystalline structure, less internal stress and comprise comparatively larger grains. In addition, the Ti2p$_{3/2}$ and O1s peaks shifted toward higher binding energy suggest that the local chemical state was influenced by the prolonged deposition duration in the film, which resulted in red shift of absorption threshold into visible-light region. Under illumination of UV-365 and RLED with wavelengths longer than 600 nm, the visible-light enabling films exhibited the best photocatalytic activity on MB degradation with the rate-constant of about 0.231 h^{-1} by UV-365. Hydrophilic conversion rate was estimated to be 8.14×10^{-3} deg^{-1} min^{-1}. The long-term UV-induced hydrophilicity of ~10° in the dark was retained up to 72 h. These are attributed to, in addition to its inherent feature on hole/electron separation by the TiO_2/ITO layered structure prepared by twin DC sputtering technique, perfectly formed crystalline structure, densely packed columnar crystals, and the surface roughness along with its enlarged surface area. The detail mechanisms on the formation of the visible-light enabling films are under further investigation in our lab.

Acknowledgements

The authors wish to thank Prof. Jen-Sue Chen of Department of Materials Science of National Cheng Kung University, Dr. Yao-Hsuan Tseng of Center for Environmental, Safety and Health Technology Development of Industrial Technology Research Institute and the engineers of MIRDC for their equipment supports and sample preparations.

References

[1] A. Fujishima, T.N. Rao, D.A. Try, J. Photochem. Photobiol. C: Photoc. Rev. 1 (2000) 1–21.
[2] S. Kumar, A.G. Fedorov, J.L. Gole, Appl. Catal. B 57 (2005) 93–107.
[3] T. Ihara, M. Miyoshi, Y. Iriyama, Appl. Catal. B: Environ. 42 (2003) 403–409.
[4] Z. Wang, W. Cai, X. Hong, X. Zhao, F. Xu, C. Cai, Appl. Catal. B: Environ. 57 (2005) 223–231.
[5] A.R. Gandhe, J.B. Fernandes, J. Solid State Chem. 178 (2005) 2953–2957.
[6] K.R. Wu, C.H. Ting, W.C. Liu, C.H. Lin, J.K. Wu, Thin Solid Films 500 (2006) 110–116.
[7] A. Mills, J. Wang, J. Photochem. Photobiol., A Chem. 127 (1999) 123–134.
[8] D.S. Rickerby, J. Vac. Sci. Technol. A 4 (November–December (6)) (1986) 2809–2814.
[9] J. Herrero, C. Guillén, Vacuum 67 (2002) 611–616.
[10] I.M. Arabatzis, T. Stergiopoulos, M.C. Bernard, D. Labou, S.G. Neophytides, P. Fala, Appl. Catal. B 42 (2003) 187–201.
[11] T.L. Hanley, V. Luca, I. Pickering, R.F. Howe, J. Phys. Chem. B 106 (2002) 1153–1160.
[12] Y. Ma, J.-B. Qiu, Y.-A. Cao, Z.-S. Quan, J.-N. Yao, Chemosphere 44 (2001) 1087–1092.
[13] S. Dohshi, M. Takeuchi, M. Anpo, Catal. Today 85 (2003) 199–206.
[14] I. Nakamura, N. Negishi, S. Kutsuna, T. Ihara, S. Sugihara, K. Takeuchi, J. Mol. Catal. A 161 (2000) 205–212.
[15] L. Miao, P. Jin, K. Kaneko, A. Terai, N. Nabatova-Gabain, S. Tanemura, Appl. Surf. Sci. 212–213 (2003) 255–263.
[16] E. McCafferty, J.P. Wightman, Appl. Surf. Sci. 143 (1999) 92–100.
[17] B. Erdem, R.A. Hunsicker, G.W. Simmons, E.D. Sudol, V.L. Dimonie, M.S. El-Aasser, Langmuir 17 (2001) 2664–2669.
[18] K. Nagaveni, M.S. Hegde, N. Ravishankar, G.N. Subbanna, G. Madras, Langmuir 20 (2004) 2900–2905.
[19] N. Sakai, A. Nakajima, T. Watanabe, K. Hashimoto, J. Phys. Chem., B 107 (2003) 1028–1035.
[20] K. Nagaveni, G. Sivalingam, M.S. Hegde, G. Madras, Appl. Catal. B 48 (2004) 83–93.
[21] R. Wang, N. Sakai, A. Fujishima, T. Watanabe, K. Hashimoto, J. Phys. Chem. B 103 (1999) 2188–2194.
[22] D. Dumitriu, A.R. Bally, C. Ballif, P. Hones, P.E. Schmid, R. Sanjinés, F. Lévy, V.I. Parvulescu, Appl. Catal. B 25 (2000) 83–92.
[23] S. Higashimoto, M. Sakiyama, M. Azuma, Thin Solid Films 503 (2006) 201–206.
[24] A. Rampaul, I.P. Parkin, S.A. O'Neill, J. DeSouza, A. Mills, N. Elliott, Polyhedron 22 (2003) 35–44.
[25] J. Bico, C. Marzolin, D. Quéré, Europhys. Lett. 55 (2) (2001) 214–220.
[26] C.S. Kuo, Y.H. Tseng, Y.Y. Li, Chem. Lett. 35 (2006) 356–357.